arXiv:1405.5855v5 [nlin.AO] 6 Jan 2016

Critical phenomena induced by intertwined dynamics on multiplex networks

Per Sebastian Skardal*[1], Vincenzo Nicosia*[2], Vito Latora[2,3], and Alex Arenas[4]

[1]Department of Mathematics, Trinity College, Hartford, CT 06106, USA

[2]School of Mathematical Sciences, Queen Mary University of London

[3]Dipartimento di Fisica ed Astronomia, Università di Catania and INFN Catania, Italy

[4]Department d'Enginyeria Informática i Matemátiques, Universitat Rovira i Virgili, 43007 Tarragona, Spain

Network-coupled dynamical processes have emerged as a powerful tool to model and study a wide variety of complex phenomena [1, 2]. Significant research has increased our understanding of many complex systems, specifically enlightening the connection and interplay between dynamics and network structure [3, 4]. However, save for a few notable exceptions [5, 6], most studies consider a single complex system acting in isolation from other processes. Here we show that new critical phenomena can be induced by intertwining different dynamical processes with distinct network topologies using a multiplex network coupling such that the different processes evolve in parallel. As an example, we study bidirectionally-coupled synchronization and transport dynamics, where the allocation of transport in one layer depends on the degree of synchronization on the other layer, and vice-versa. Multiplexity induces, at the same time, a transition to a heterogeneous distribution of allocations and the emergence of a switch-like bistability in the synchronization dynamics. Our results can find applications in cases where synchronization is subject to the transport of available resources, such as in the brain [7] or in power networks [8].

The study of collective dynamical processes on complex networks in recent years has shed a great deal of light on a wide range of physical, biological, and social phenomenon including syn-

*These authors contributed equally to this work.

chronization [9], spreading [10], transport [11], and cascades [12]. Of particular interest in these works is the interplay between dynamics and network structure – in many cases the nature of the collective dynamics reveals structural information about the network [13, 14] and the underlying networks structure has a strong effect on the emerging dynamics [15]. Our understanding of the fundamental mechanisms driving these phenomena provide a solid foundation for modeling, predicting, and controlling dynamical processes in the real world, however the majority of studies ignore an important piece: connections between *different* dynamical processes. In this Letter we propose a framework for connecting different dynamical processes through interconnected multiplex networks, generating a new level of complexity through the intertwined nature of the system. Moreover, we demonstrate with a specific example that this new level of complexity can give rise to emergent critical phenomena.

To couple two or more distinct dynamical processes, each taking place on a different network, we employ a multiplex network, i.e., a network structure consisting of M layers, where each layer provides the structure for a different dynamical process [16]. Each layer contains N nodes, such that a one-to-one correspondence between nodes in different layer exists, and importantly, both the structural topology and nature of connections represented by links may differ in different layers [17]. The network in layer m is represented by the adjacency matrix $A^{[1]} = \left\{a_{ij}^{[m]}\right\}$, such that $a_{ij}^{[m]} = 1$ if a link exists between nodes i and j in the m-th layer, and otherwise $a_{ij}^{[m]} = 0$. The dynamics on each layer evolves as normal – in accordance with its own state and the state of its network neighbors (in the same layer) – but also in accordance with the dynamics in other layers. In general, we allow the parameters of the dynamics of at given node in a given layer to depend on the dynamical state of the corresponding node in the other layers. Thus, each dynamical process is bi-directionally coupled with the other dynamical processes in such a way that both the dynamics and network structure of each process affects each other dynamical process in the multiplex. We make such a formalism explicit in Appendix A.

As an illustrative concrete example of how such multiplex dynamical coupling between two networked dynamical processes gives rises to the emergence of novel phenomena, unobserved when the two dynamics are uncoupled, we will describe and provide an analysis for a system of intertwined synchronization and transport dynamics. This yields a two-layered multiplex as depicted in Figure 1(a): one layer supports a process of synchronization, while the other supports a process of transport. We also denote the node degree in the synchronization (transport) layer as: $k_i^{[1]} = \sum_{j=1}^{N} a_{ij}^{[1]}$ ($k_i^{[2]} = \sum_{j=1}^{N} a_{ij}^{[2]}$). The synchronization dynamics is governed by the Kuramoto model [18], such that the state of node i at layer 1 is described by the phase $\theta_i \in [0, 2\pi)$ of an oscillator which evolves according to

$$\dot{\theta}_i = \omega_i + \lambda \sum_{j=1}^{N} a_{ij}^{[1]} \sin(\theta_j - \theta_i), \tag{1}$$

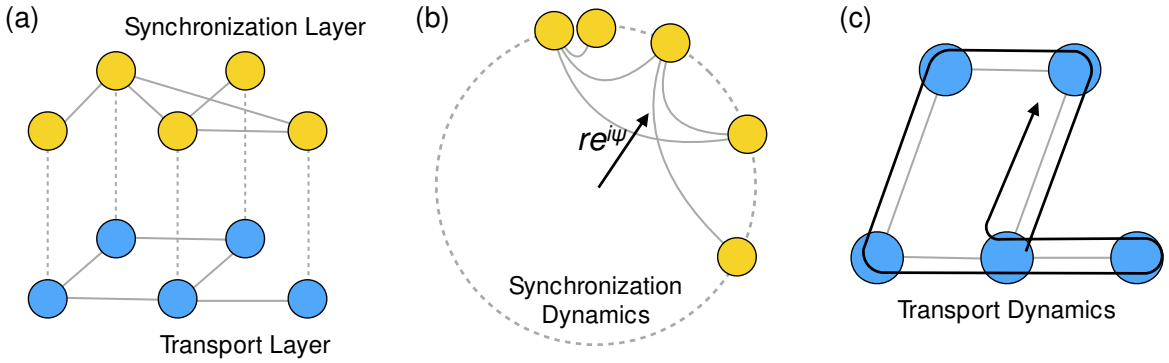

Figure 1: **Model setup.** (a) An example two-layer multiplex of $N = 5$ nodes with a synchronization layer (top) and transport layer (bottom). (b) The synchronization dynamics take place on the synchronization layer, evolve according to Equation (1), and is measured using the order parameter r. (c) The transport dynamics consist of random walkers traversing the transport layer according to Equation (2). The two dynamical processes are intertwined by the co-dependent evolution of the natural frequencies and the transition probabilities, as described in Equations (3)–(4).

where ω_i is the natural frequency of the oscillator i and λ is the global coupling strength. The degree of global synchronization is measured using the typical Kuramoto order parameter r defined by the complex number $re^{i\psi} = \frac{1}{N}\sum_{j=1}^{N} e^{i\theta_j}$ which represents the centroid of all oscillators places on the complex unit circle. On the other hand, the transport dynamics is modeled by a continuum of random walkers traversing the second layer. Specifically, the state y_i of the node at the transport layer is described by the fraction $p_i(t) \in [0, 1]$ of random walkers at node i at time t, which evolves according to:

$$p_i(t + \delta t) = \sum_{i=1}^{N} \pi_{ij} p_j(t) \qquad \pi_{ji} = \frac{a_{ij}^{[2]} f_j^{\alpha}}{\sum_l a_{il}^{[2]} f_l^{\alpha}} \tag{2}$$

where π_{ji} is the probability of moving from node i to node j in a unit time step, and we have assumed the random walk is biased on the node property f_j, with a tunable bias exponent α [19]. In principle, the timestep δt represents a new parameter and an effective timescale in the model. To complete the model, we now assume a bi-directional dependence between the two dynamical processes. Specifically, we utilize the inter-layer links, allowing the oscillator dynamics at node i in the synchronization layer to depend on the random walker dynamics at node i in the transport layer, and vice-versa. The coupling between the two dynamical processes is mediated by the functional dependence of the parameters of each process on the state of the other process. In particular, we allow the oscillators' natural frequencies and the random walkers' transition probabilities to evolve dynamically as a function of the fraction of walkers and of the level of synchronization at a node, respectively. First, we assume that the natural frequencies ω_i, $i = 1, 2, \ldots, N$, relax to values

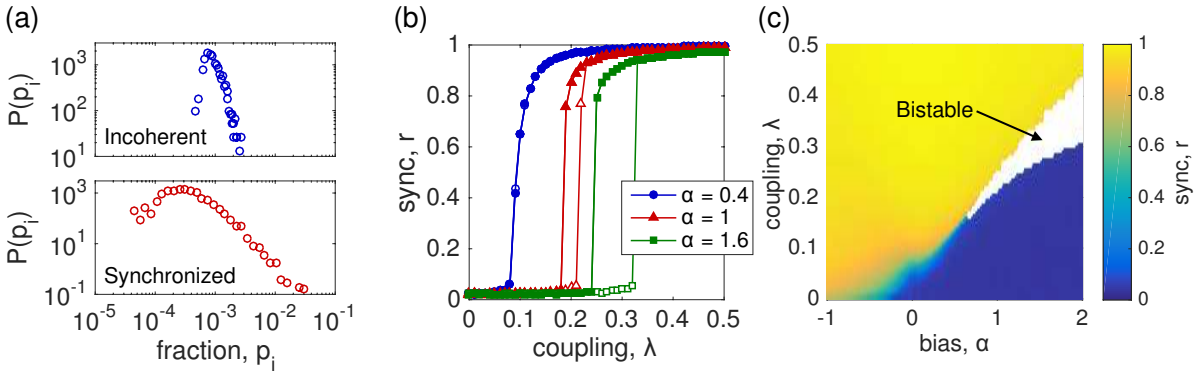

Figure 2: **Spontaneous synchronization fostered by intertwined dynamics.** (a) Distribution $P(p_i)$ of steady-state random walker fractions p_i for an incoherent (top, blue) and synchronized (bottom, red) states. (b) Synchronization profiles r vs λ for biasing exponents $\alpha = 0.4$, 1, and 1.6 (blue, red, and green, respectively). (c) Synchronization phase space for the coupling λ and biasing exponent α. The bistable region is colored white. Networks are of size $N = 1000$ with $\gamma = 3$ and $\langle k^{[1]} \rangle = \langle k^{[2]} \rangle = 10$ and timescales are set $\tau_\omega, \tau_f = 0$ and $\delta t = 1$.

proportional to the fraction of random walkers at node i in the transport layer,

$$\tau_\omega \dot{\omega}_i = N p_i(t) - \omega_i, \tag{3}$$

where τ_ω gives the timescale for the relaxation. Next, we define the dynamic strength of node i, $s_i^{\text{dyn}} = \max[\epsilon, r_i \cos(\psi_i - \theta_i)]$ where $0 < \epsilon \ll 1$ and $r_i e^{i\psi_i} = \sum_j a_{ij}^{[1]} e^{i\theta_j}$ is the local synchronization order parameter for oscillator i, such that s_i^{dyn} measures the degree to which oscillator i is synchronized with its neighbors. We assume the quantities f_i evolve according to

$$\tau_f \dot{f}_i = s_i^{\text{dyn}} - f_i. \tag{4}$$

Thus, f_i relaxes to the dynamic strength of oscillator i with a timescale τ_f, and therefore the random walk described by the transition probabilities in Equation (2) is biased towards (away from) strongly-synchronized nodes for positive (negative) values of α.

To illustrate the effects of intertwining the two dynamical processes through the model described above, we consider a network of size $N = 1000$ whose synchronization layer has a scale-free network topology built with the configuration model [20] with degree distribution $P\left(k^{[1]}\right) \propto \left(k^{[1]}\right)^{-\gamma}$ above an imposed minimum degree $k_0^{[1]}$, and whose transport layer topology is Erdős-Rényi [21] with link probability p. The mean degrees are thus given by $\langle k^{[1]} \rangle = \frac{\gamma-1}{\gamma-2} k_0^{[1]}$ and $\langle k^{[2]} \rangle = p(N-1)$. In particular, we choose a SF network for the synchronization layer given the prevalence of such topologies in real networks varying from the World Wide Web to power grids [22]. Setting $\gamma = 3$ and $\langle k^{[1]} \rangle = \langle k^{[2]} \rangle = 10$, we simulate the model for various biasing parameters α as the coupling strength λ is adiabatically increased and then decreased, and summarize the results in Figure 2. Timescales

are chosen $\tau_\omega, \tau_f = 0$, corrsponding to instantaneous relaxation in Eqs. (3) and(4), and $\delta t = 1$ for the random walk in Eq. (2). In Figure 2(a) we plot the distribution $P(p_i)$ of steady-state random walker fractions p_i while the system is in an incoherent state (top, blue), and a synchronized state (bottom, red). While the values of p_i are relatively homogeneous in the incoherent state (note the linear horizontal axis), in the synchronized state the distribution is very heterogeneous, spanning several decades (note the logarithmic horizontal axis). In Figure 2(b) we plot the synchronization profiles r vs λ for $\alpha = 0.4$, 1, and 1.6 (blue circles, red triangles, and green squares respectively), where for $\alpha = 0.4$ we observe the typical continuous transition of the Kuramoto model while, for $\alpha = 1$ and 1.6, the forward and backward parts of the profiles reveal the emergence of a bistability in the form of a hysteresis loop. Finally, in Figure 2(c) we explore the α, λ parameter space in more detail, plotting the r as a function of the two parameters, and denoting the bistable region in white – which emerges at $\alpha \approx 0.7$ and widens as α is increased.

Our results show that the multiplex coupling of random walk and synchronization dynamics gives rise to the emergence of novel critical phenomena in both layers, which is unexpected in the uncoupled systems. In the transport layer, we observe a transition from a homogeneous to a heterogeneous distribution of the random walkers throughout the network, according to whether the oscillators in the opposite layer are incoherent or synchronized. Concurrently, when the random walkers are sufficiently biased towards nodes that are strongly synchronized, the heterogenous distribution of random walkers fosters the emergence of switch-like explosive synchronization [23] in the synchronization layer. The resulting phase diagram exhibits three phases (incoherent, bistable, and synchronized) that converge at a critical point.

We now demonstrate that, despite the inherent intricacy of the model, analytical progress can be made in describing its novel dynamics. In particular, we search for a stationary state in the system where the random walker probabilities and local order parameters reach a stationary state, $p_i = p_i^*$ and $r_i = r_i^*$. A steady-state analysis can then be carried out for both the transport and synchronization dynamics, which we detail in Appendices B and C. In particular, we find that the fraction of random walkers p_i^* depends on whether the synchronization dynamics are incoherent or synchronized:

$$p_i^* \propto \begin{cases} k_i^{[2]} & \text{if } r \approx 0 \\ \left(k_i^{[1]}\right)^\alpha k_i^{[2]} \langle \left(k^{[1]}\right)^\alpha \rangle_i & \text{if } r \approx 1. \end{cases} \tag{5}$$

Also, the global order parameter r can be written implicitly in terms of the collective frequency $\Omega = \langle \omega \rangle$ and the joint degree-frequency distribution $P(k, \omega)$:

$$r = \frac{1}{\langle k^{[1]} \rangle} \iint_{|\omega - \Omega| \leq \lambda r k^{[1]}} P(k^{[1]}, \omega) k^{[1]} \sqrt{1 - \left(\frac{\omega - \Omega}{\lambda r k^{[1]}}\right)^2} d\omega dk^{[1]}, \tag{6}$$

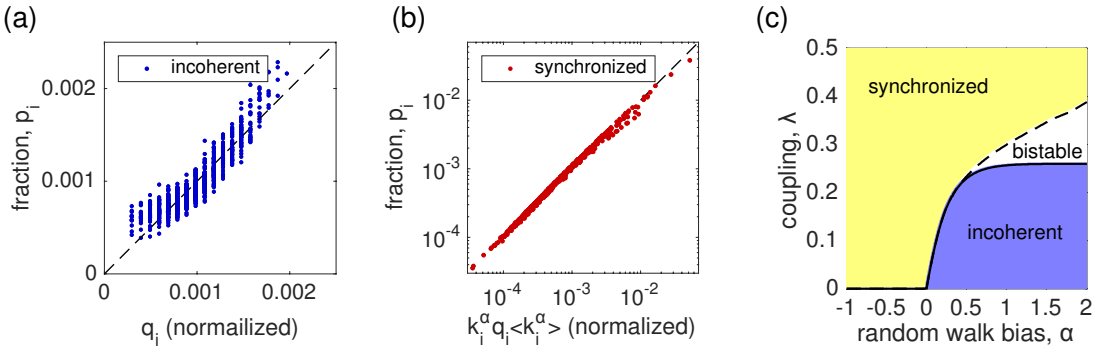

Figure 3: **Analytical description of macroscopic dynamics.** Steady-state random walker fractions p_i for (a) an incoherent state vs. $k_i^{[2]}$ (normalized) and (b) a synchronized state vs. $(k_i^{[1]})^\alpha k_i^{[2]} \langle (k^{[1]})^\alpha \rangle_i$. (c) Analytically obtained phase space for λ and α. Networks are of size $N = 1000$ with $\gamma = 3$ and $\langle k^{[1]} \rangle = \langle k^{[2]} \rangle = 10$.

In Figure 3 we demonstrate these analytical results. First, we plot the steady-state random walker fractions p_i vs the normalized predictions in Equation (5) for an incoherent and synchronized state in Figures 3(a) and (b), respectively, and dashed black lines indicating perfect agreement are plotted to guide the eye. In Figure 3(c) we plot the synchronization phase space for λ and α as computed using Equation (6). We note a strong agreement both qualitatively and quantitatively between our simulations and analytical predictions.

In this Letter we have introduced a framework for studying systems consisting of several intertwined dynamical processes. Our approach uses multiplex networks to mutually couple dynamics of different nature, and our results show that novel critical phenomena, unobserved in each of the dynamical systems taken in isolation, emerges because of the multiplex coupling. As an example with potentially important practical applications, we have studied in detail a system of intertwined synchronization and transport dynamics, finding that the bidirectional coupling between the two layers creates new critical behaviors. Namely, the distribution of random walkers in the transport network changes from homogeneous to heterogeneous according to whether the synchronization dynamics is incoherent or synchronized, respectively, and, at the same time, the heterogeneous distribution of random walkers is responsible for the appearance of a bistable state and critical point in the synchronization dynamics. Despite the significant jump in complexity over other synchronization and transport network models studied to date [24, 25], we have demonstrated that analytical results can in fact be obtained, and reproduce quite well the observed novel phenomenology.

The choice of the specific model studied here was motivated by the important role that synchronization and transport play in a wide range of natural and man-made systems [26, 27], and the switch-like transition we have found mirrors various bistabilities empirically observed in physics, biology and neuroscience [28, 29, 30]. We believe that further studies of other intertwined dynam-

ical processes will result in more robust models of real systems, possibly uncovering other novel phenomena induced by the multiplex coupling of different dynamical processes.

Appendix

A General formalism for intertwined dynamics

Here we briefly discuss a general formalism for modeling two or more distinct, intertwined dynamical processes using a multiplex network. For simplicity, we consider the case of only two intertwined dynamical processes, however we emphasize that such a formalism can be easily extended to an arbitrary number. We therefore consider a multiplex consisting of N nodes on $M = 2$ layers. The topology of the first and second layer are described using the adjacency matrices $A^{[1]} = \{a_{ij}^{[1]}\}$ and $A^{[2]} = \{a_{ij}^{[2]}\}$, respectively, such that $a_{ij}^{[1]} = 1$ ($a_{ij}^{[2]} = 1$) if a link exists between nodes i and j in the first (second) layer, and otherwise $a_{ij}^{[1]} = 0$ ($a_{ij}^{[2]} = 0$). Next, we denote the state of the dynamics at node i in the first and second layer by x_i and y_i, respectively. The dynamics of each x_i and y_i are then governed by a system of equations of the form

$$\begin{cases} \dot{x}_i = F_{\chi_i}(\mathbf{x}, A^{[1]}) & \text{(layer 1)} \\ \dot{y}_i = G_{\Upsilon_i}(\mathbf{y}, A^{[2]}) & \text{(layer 2)} \end{cases} \qquad i = 1, 2, \dots N, \tag{7}$$

where $\mathbf{x} = [x_1, x_2, \dots, x_N]^T \in \mathbb{R}^N$ and $\mathbf{y} = [y_1, y_2, \dots, y_N]^T \in \mathbb{R}^N$. Thus, the dynamical evolution of the two network processes is ruled respectively by the functions F_χ and G_Υ which are functions of the layer-specific state vector and network topology, and where χ and Υ represent the parameters for the dynamics of x and y, respectively. so that the state x_i (y_i) of node i of the first (second) layer is a function of the state $\mathbf{x}$ ($\mathbf{y}$) and of the topology $A^{[1]}$ ($A^{[2]}$) of the first (second) layer. The key ingredient that connects the two dynamical processes is provided by the nature of the correspondence *between layers*. To provide this coupling, we allow the parameters χ_i and Υ_i depend on the state of the dynamics in the *opposite* layer. Specifically, we allow χ_i and Υ_i evolve according to

$$\begin{cases} \dot{\chi}_i = f(\chi_i, y_i) \\ \dot{\Upsilon}_i = g(\Upsilon_i, x_i) \end{cases} \qquad i = 1, 2, \dots N, \tag{8}$$

thus completing the bi-directional coupling between the two dynamical processes.

We note briefly that, although both equations in (7) are written in the form of ordinary differential equations, other variations can also be used. In particular, one or more of the evolution equations can be described in terms of a disctrete dynamical system, as we have used for the transport dynamics [i.e., Eq. (2)].

B Derivation of the biased random walker stationary distribution

Here we follow Ref. [19] and derive the stationary distribution of random walkers $\boldsymbol{p}^*$ given by Eq. (5) for the biased random walker process defined by the transition probabilities in Eq. (2). Eq. (2) is a specific case of the more generic class of random walks defined by the rule:

$$\pi_{ji} = \frac{a_{ij}^{[2]} g_j}{c_i}, \tag{9}$$

where g_j is an arbitrary nodal property for node j and $c_i = \sum_{j=1}^{N} a_{ij}^{[2]} g_j$. Denoting the probability of moving from node i to node j in t time steps $P_{i\to j}(t)$, we find that

$$P_{i\to j}(t) = \sum_{l_1, l_2, \ldots, l_{t-1}} \pi_{j l_{t-1}} \times \pi_{l_{t-1} l_{t-2}} \times \cdots \times \pi_{l_1 i}, \tag{10}$$

where $l_1, \ldots, l_{t-1}$ are the indices of nodes traversed by the walker when going from i to j. Assuming that the graph on the transport layer is undirected (i.e., $a_{ij}^{[2]} = a_{ji}^{[2]}$), it follows that the ration of the probability of moving from i to j to the probability of moving from j to i in t timesteps is given by

$$\frac{P_{i\to j}(t)}{P_{j\to i}(t)} = \frac{g_j c_j}{g_i c_i}. \tag{11}$$

Next we search for a stationary state whereby the probability p_i^* of a walker occupying node i is equal to $P_{l\to i}(t)$ for all l and $t > 0$. Substituting the stationary probabilities and rearranging yields

$$g_i c_i p_j^* = g_j c_j p_i^*. \tag{12}$$

Summing both sides of Eq. (12) over j and rearranging, we then obtain

$$p_i^* = \frac{g_i c_i}{\sum_{j=1}^{N} g_j c_j}. \tag{13}$$

Finally, we set the arbitrary nodal value g_i equal to the biasing value f_i^α we obtain the stationary state of the random walker process given by

$$p_i^* = \frac{f_i^\alpha \sum_{j=1}^{N} a_{ij}^{[2]} f_j^\alpha}{\sum_{l=1}^{N} f_l^\alpha \sum_{j=1}^{N} a_{lj}^{[2]} f_j^\alpha}. \tag{14}$$

To complete the analysis, we next assume that the biasing values f_i defined by Equation (4) come to a steady-state. Such a steady-state is defined by $\dot{f}_i = 0$, yielding $f_i = s_i^*$, where s_i^* represents the steady-state dynamical strength s_i^{dyn} in the synchronization as defined by the synchronization dynamics. (We note that such a steady-state value s_i^* is valid provided that the network is large

enough so that finite-size fluctuations remain sufficiently small.) Since the steady-state dynamical strength is defined $s_i^* = \max[\epsilon, r_i^* \cos(\theta_i^* - \theta_i^*)]$ and the local order parameter can be approximated $r_i^* \approx k_i^{[1]} r^*$, it follows that at steady-state we have

$$f_i^* = s_i^* \approx r k_i^{[1]}, \tag{15}$$

Inserting this into Equation (14), we finally obtain

$$p_i^* \propto \begin{cases} k_i^{[2]} & \text{if } r \approx 0 \\ \left(k_i^{[1]}\right)^{\alpha} k_i^{[2]} \langle \left(k^{[1]}\right)^{\alpha} \rangle_i & \text{if } r \approx 1, \end{cases} \tag{16}$$

as in Equation (5).

C Derivation of the synchronization self-consistency equation

Here we derive, from the governing synchronization dynamics in Eq. (1), the self consistency condition given in Eq. (6) using a heterogeneous mean-field approach. In particular, we will approximate the entries of the adjacency matrix A using nodal degrees, specifically

$$a_{ij}^{[1]} \approx \frac{k_i^{[1]} k_j^{[1]}}{N \langle k^{[1]} \rangle}, \tag{17}$$

where $\langle k^{[1]} \rangle = N^{-1} \sum_j k_j^{[1]}$ is the mean degree in the synchronization layer. We also introduce a modified order parameter,

$$\tilde{r} e^{i\tilde{\psi}} = \frac{1}{N \langle k^{[1]} \rangle} \sum_{j=1}^{N} k_j^{[1]} e^{i\theta_j}, \tag{18}$$

which is similar to the typical order parameter, except for a re-weighting of the angles according to degree. We note that, just like r, the modified order parameter $\tilde{r}$ varies between zero and one, and tends to be a very strong approximation to r. We introduce the modified order parameter because of its utility in the analysis of the dynamics. Along with the the mean-field approximation of A [i.e., Eq. (17)], Eq. (18) allows us to simplify the governing dynamics in the synchronization layer to

$$\dot{\theta}_i = \omega_i + \lambda \tilde{r} k_i^{[1]} \sin(\tilde{\psi} - \theta_i). \tag{19}$$

Next, we search for a synchronized state by first noting that for a strongly synchronized population, where each oscillator becomes entrained, the collective frequency Ω of the population is

given by the mean natural frequency, i.e., $\Omega = \langle\omega\rangle = N^{-1}\sum_j \omega_j$. Thus, an oscillator that becomes entrained with the rest of the population evolves with a velocity of $\dot{\theta}_i = \Omega$. After entering the appropriate rotating frame $\theta_i \mapsto \theta_i + \Omega t$ and inspecting Eq. (19), it is easy to see that an oscillator i becomes entrained, or locked, if and only if it satisfies

$$|\omega_i - \Omega| \leq \lambda \tilde{r} k_i^{[1]}, \tag{20}$$

and otherwise it continually "drifts" past the synchronized population. In particular, a locked oscillator i then comes to equilibrium at

$$\theta_i = \arcsin\left(\frac{\omega_i - \Omega}{\lambda \tilde{r} k_i^{[1]}}\right). \tag{21}$$

To classify the degree of synchronization we inspect the modified order parameter $\tilde{r}e^{i\tilde{\psi}}$. First, we note that with a suitable shift initial conditions we may set the mean angle $\psi = 0$, so expanding the exponential and keeping the real part (since the imaginary part must be zero) yields

$$\tilde{r} = \frac{1}{N\langle k^{[1]}\rangle}\sum_{j=1}^{N} k_j^{[1]} \cos\theta_j. \tag{22}$$

Neglecting the effect of drifting oscillator on the order parameter, we sum over the locked population and insert Eq. (21) into Eq. (22) to obtain

$$\tilde{r} = \frac{1}{N\langle k^{[1]}\rangle}\sum_{|\omega_j - \Omega| \leq \lambda \tilde{r} k_j^{[1]}} k_j^{[1]} \sqrt{1 - \left(\frac{\omega_j - \Omega}{\lambda \tilde{r} k_j^{[1]}}\right)^2}. \tag{23}$$

Finally, for large networks the sum in Eq. (23) can be converted to an integral using the joint distribution $P(k^{[1]}, \omega)$:

$$\tilde{r} = \frac{1}{\langle k^{[1]}\rangle}\int_{|\omega - \Omega| \leq \lambda \tilde{r} k^{[1]}} k^{[1]} \sqrt{1 - \left(\frac{\omega - \Omega}{\lambda \tilde{r} k^{[1]}}\right)^2} d\omega dk^{[1]}, \tag{24}$$

which matches Eq. (6) after approximating $r \approx \tilde{r}$.

References

[1] Strogatz, S. H. Exploring complex networks. *Nature* **410**, 268–276 (2001).

[2] Newman, M. E. J. The structure and function of complex networks. *SIAM Rev.* **45**, 167–256 (2003).

[3] Boccaletti, S., Latora, V., Moreno, Y., Chavez, M. & Hwang, D. U. Complex networks: structure and dynamics. *Phys. Rep.* **424**, 175–308 (2006).

[4] Arenas, A., Díaz-Guilera, A., Kurths, J., Moreno, Y. & Zhou, C. Synchronization in complex networks. *Phys. Rep.* **469**, 93–153 (2008).

[5] Buldyrev, S. V., Parshani, R., Paul, G., Stanley, H. E. & Havlin, S. Catastrophic cascade of failures in interdependent networks. *Nature* **464**, 1025–1028 (2010).

[6] Granell, C., Gomez, S. & Arenas A. Dynamical interplay between awareness and epidemic spreading in multiplex networks. *Phys. Rev. Lett.* **111**, 128701 (2013).

[7] Varela, F., Lacjaux, J.-P., Rodriguez, E. & Martinerie, J. The brainweb: Phase synchronization and large-scale integration. *Nat. Rev. Neurosci.* **2**, 229–239 (2001).

[8] Motter, A. E., Myers, S. A., Anghel, M. & Nishikawa, T. Spontaneous synchrony in power-grid networks. *Nat. Phys.* **9**, 191–197 (2013).

[9] Dörfler, F., Chertkov, M., and Bullo, F. Synchronization in complex oscillator networks and smart grids. *Proc. Natl. Acad. Sci. U.S.A.* **110**, 2005–2010 (2013).

[10] Pastor-Satorras, R. & Vespignani, A. Epidemic spreading in scale-free networks. *Phys. Rev. Lett.* **86**, 3200 (2001).

[11] Noh, J. D. & Rieger, H. Random walks on complex networks. *Phys. Rev. Lett.* **92**, 118701 (2004).

[12] Larremore, D. B., Shew, W. L. & Restrepo, J. R. Predicting criticality and dynamic range in complex networks: effects of topology. *Phys. Rev. Lett.* **106**, 058101 (2011).

[13] Arenas, A., Díaz-Guilera, A. & Pérez-Vicente, C. J. Synchronization reveals topological scales in complex networks. *Phys. Rev. Lett.* **96**, 114102 (2006).

[14] Rosvall, M. & Bergstrom, C. T. Maps of random walks on complex networks reveal community structure. *Proc. Natl. Acad. Sci.* **105**, 1118–1123 (2008).

[15] Nishikawa, T., Motter, A. E., Lai, Y.-C. & Hoppensteadt, F. C. Heterogeneity in oscillator networks: are smaller worlds easier to synchronize? *Phys. Rev. Lett.* **91**, 014101 (2003).

[16] De Domenico, M., Solé-Ribalta, A., Cozzo, E., Kivelä, M.,Moreno, Y., Porter, M. A., Gomez, S. & Arenas, A., Mathematical formulation of multi-layer networks. *Phys. Rev. X* **3**, 041022 (2013).

[17] Kivelä, M., Arenas, A., Barthelemy, M., Gleeson, J. P., Moreno, Y. & Porter, M. A. Multilayer networks. *J. Complex Netw.* **2**, 203–271 (2014).

[18] Y. Kuramoto, Y. Chemical Oscillations, Waves, and Turbulence (Springer, 1984).

[19] Gómez-Gardeñes, J. & Latora, V. Entropy rate of diffusion processes on complex networks. *Phys. Rev. E* **78**, 065102(R) (2008).

[20] Molloy, M. & Reed, B. Critical point for random graphs with a given degree sequence. *Random Struct. Algor.* **6**, 161–180 (1995).

[21] Erdős, P. & Rényi, A. On the evolution of random graphs. *Publ. Math. Inst. Hung. Acad. Sci.* **5**, 17–61 (1960).

[22] Barabási, A.-L. & Albert, R. Emergence of scaling in random networks. *Science* **286**, 509–512 (1999).

[23] Gómez-Gardeñes, J., Gómez, S., Arenas, A. & Moreno, Y. Explosive synchronization transitions in scale-free networks. *Phys. Rev. Lett.* **106**, 128701 (2011).

[24] Restrepo, J. G., Ott, E. & Hunt, B. R. Onset of synchronization in large networks of coupled oscillators. *Phys. Rev. E* **71**, 036151 (2005).

[25] Lambiotte, R., Sinatra, R., Delvenne, J.-C., Evans, T. S., Barahona, M. & Latora, V. Flow-graphs: Interweaving dynamics and structure. *Phys. Rev. E* **84**, 017102 (2011).

[26] Skardal, P. S. & Arenas, A. Control of coupled oscillator networks with application to microgrid technologies. *Sci. Adv.* **1**, e1500339 (2015).

[27] Gleich, D. F. PageRank beyond the web. *SIAM Rev.* **57**, 321–363 (2015).

[28] Martens, E. A., Thutupalli, S., Fourrière, A. & Hallatschek, O. Chimer states in mechanical oscillator networks. *Proc. Natl. Acad. Sci. U.S.A.* **110**, 10563–10567 (2013).

[29] Brandman, O., Ferrell, J. E., Li, R. & Meyer, T. Interlinked fast and slow positive feedback loops drive reliable cell decisions. *Science* **310**, 496–498 (2005).

[30] Deco, G., Jirsa, V. K. & McIntosh, A. R. Resting brains never rest: computational insights into potential cognitive architectures. *Trends. Neurosci.* **36**, 268–274 (2013).